Numerical Simulation of the Flow Pulsations Origin in Cascades of the Rear Blade Rows in a Gas Turbine Axial Compressor Using Low Calorific Fuel

Vaclav Cyrus
AHT Energetics Ltd.,
Podnikatelska 550, Prague-Bechovice,
Prague 19011, Czech Republic
e-mail: cyrus.aht@iol.cz

Jiri Polansky
West Bohemia University,
Universitni 8, Pilsen 30616
e-mail: polansky@kke.zcu.cz

Fatigue failure of the last three stator rows vanes (S17, EGV1, and EGV2) in the 17 stage gas turbine axial compressor occurred in the power plant where low calorific fuel syngas, was used. Causes of this dangerous phenomenon were flow pulsations with the frequency of 380–400 Hz that were found by the experimental investigation of the duty gas turbine. Mechanism of the flow unsteadiness origin was studied with the help of flow simulations in the 2D stator cascade system. Three numerical experiments were carried out. The first experiment investigated the flow simulation in the stator cascade system with a steady undisturbed inlet flow with increased turbulence intensity. Obtained data did not meet the standards of the actual compressor operations. In the remaining two numerical experiments, a purposely designed rotor cascade was located in front of the stator cascades. Shedding of vortex structures from the cascade profile surfaces at positive incidence angles is responsible for the flow pulsation origin. The interaction of rotor wakes/stator S17 cascade plays an important role in the investigated phenomenon, as follows from CFD data. Aerodynamic loading of both cascades is equal in the second group of numerical experiments. Computed results were in good qualitative agreement with the experimental ones. As the flow in rotor cascade was not separated, owing to the different aerodynamic loading of rotor and stator S17 cascades, the vortices shedding in stator cascade S17 had a significantly higher frequency of $f=2200-2300$ Hz than in other investigated cases. [DOI: 10.1115/1.3153306]

1 Introduction

Blade failures in the rear part of a gas turbine axial compressor often occur if a low calorific fuel is used, e.g., syngas produced by coal [1], biomass, and a heavy coal/hydrogen gasification. Such outcome is described in several publications [2,3]. Explanation of these failures is connected to the fact that syngas produced in the gasification plants has 3–5 times lower calorific value than natural gas [4]. Consequently, more fuel is needed to reach the equivalent thermal input in the combustion chamber. As a result, the turbine inlet pressure must increase and the pressure rise is required to be delivered by the compressor, thus, the working point of the compressor is shifted to the surge point. Subsequently, increased gap of the stage operating point from its design position occurs along the turbomachine axis. It means that large regions of stalled flow on the vane surface due to the positive incidence angles will exist in the last blade rows. Generally, the vortex structure shedding from blades surfaces is assumed as the cause of blade failures. However, the aerodynamic loading of the blade elements last rows of compressor is below the critical limit for the cascade stall. Turbocompressor works in a stable regime without the rotating stall and surge. As of yet, the origin of such dangerous phenomenon has not been investigated in great detail.

Our experiments were carried out on a heavy duty gas turbine, working in a combined cycle with the gasification of brown coal, in Vresova power station located in Northern Bohemia [3,5].

The last three stator rows vanes' damage (17th stator, exit guide vanes—EGV1 and EGV2) due to the high cycle fatigue was caused by the flow pulsations with the frequency values of 380–400 Hz. The basic theory on the flow unsteadiness origin was verified by means of introductory numerical flow simulations in the last stator rows 2D cascades in the midspan annulus area. Acquired results confirmed vortices shedding from the stator vanes surfaces. However, a more detailed explanation of this dangerous phenomenon was required.

Unsteady viscous and 3D flow in the multistage axial compressor blading is extremely complex, mainly due to the blade rows' interactions. Tan, in Refs. [6,7], explained sources of the unsteady flows in subsonic compressors working in stable conditions without the surge and rotating stall. He distinguishes between the potential and vortical interactions. The potential interaction is associated with the influence of the pressure field of individual blades on the other blade rows. Vortical interactions involve wakes and vortices shedding from the upstream blade rows. We can consider three types: wakes, tip leakage vortex, and streamwise vortices in channels between adjacent blades without the tip clearance. These effects are described in Refs. [8–12].

Detailed insight into the blade rows interaction effects, in a low speed four stage axial compressor at TU Dresden, is given in papers presented by Mailach and Vogeler [10]. Selected results of the flow field measurements are introduced at the design and off-design operating points. However, no flow pulsations were observed in blading near the stability limit. Unsteady boundary layer developments on the rotor and stator blade surfaces of the first and third stages were presented. The transition of the laminar boundary layer into the turbulent one is clearly described. Transition process is strongly affected by wakes of periodically passing blades.

Manuscript received March 10, 2009; final manuscript received April 17, 2009; published March 25, 2010. Review conducted by David Wisler. Paper presented at the ASME Turbo Expo 2008: Land, Sea and Air (GT2008), Berlin, Germany, June 9–13, 2008.

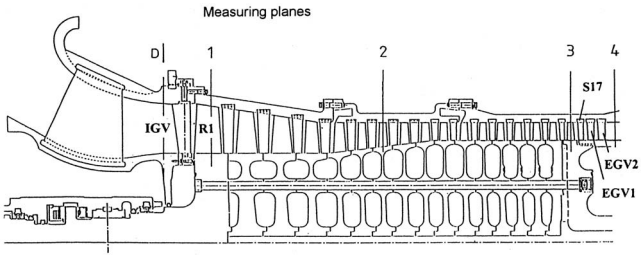

Fig. 1 Axial compressor

Fig. 2 Stator vane damage

Much research into the turbomachinery boundary layers has been accomplished in past years; refer to Refs. [13,14]. The role of the negative jet effect, originated by the movement of the chopped wake in the blade passage, in the unsteady boundary layer development on the blade surface is explained in several publications; refer to Refs. [7,10]. There have been fewer publications investigating high speed turbocompressors; refer to Ref. [15].

The present paper first summarizes our experimental data on the flow pulsation origin obtained in the 17 stage gas turbine axial compressor. A key part of the paper is devoted to the flow simulation in a 2D cascade system of the last three stator vane rows in the middle part of the annulus height. The paper's aim was the clarification of the flow pulsations origin in cascades of the last blade rows in the gas turbine axial compressor. As far as we can ascertain, there is no detailed flow mechanism description of this harmful phenomenon in available literature.

Three numerical experiments were carried out. The first experiment investigated the flow simulation in the stator cascade system with steady undisturbed inlet flow with increased flow turbulence intensity. In the remaining two numerical experiments, the rotor cascade was located in front of the stator cascade system in order to study the rotor/stator blade rows' interaction effect on the flow unsteadiness origin. Two cases were investigated. First, the aerodynamic loading of the rotor and 17th stator cascades was considered to be approximately same. Second, the flow case with lower aerodynamic loading of the rotor cascade, to compare it with the 17th stator cascade, was studied. Different values of the flow pulsations frequency were found in the two groups of simulation experiments. Numerical data analysis revealed the principal role of the rotor/stator cascade's interaction in the flow unsteadiness appearance in the rear part of the gas turbine compressor blading using syngas as fuel.

2 Summary of the Experimental Results Obtained in a Gas Turbine Axial Compressor

Figure 1 shows a meridional view of the seventeen stages General Electric M 9001E axial compressor. Compressor mass flow rate is adjusted by turning the inlet guide vanes (IGVs). Air flow is turned in the axial direction by tandem exit guide vane rows EGV1 and EGV2. Turbomachine revolutions are $n=3000$ 1/min. The geometry of compressor flow path was determined from a meridional view of the turbomachine in a scale of 1:10 (Fig. 1). Outer and inner diameters of rear part of axial compressor blading (R17, S17, EGV1, and EGV2) are constant with a hub/tip ratio of 0.85. External diameter is 1.88 m. The exact geometry of last three stator vane rows was known. This was not true for 17th rotor blade row. The compressor casing is split into two parts. Stator vanes are inserted into the casing grooves. The last three stator rows had clearances between vane tips and hub surface. Aspect ratio $AR=h/c$ of these vanes is $AR=3.0$ ($h=140$ mm).

At the casing split line two types of vane attachment were monitored. In the first case the vane forces act on vane shanks with a very rigid vane groove attachment. Thus the vane's first natural frequency is especially close to the values established by the laboratory based dedicated measurement electromagnetic excitation device. We found that for all vanes, S17, EGV1, and EGV2, values of the first natural frequency were in the range of 325–345 Hz. Cracks and fractures were found on the stator vane root surfaces.

In the second case the vane shank attachment in grooves, near the split line, was not rigid. We found a clearance between vane shanks and the split line. Consequently, magnitude of the first natural frequency values of stator vanes was lower than that obtained by the dedicated measuring apparatus. Here, a high frequency fatigue damage of vane shanks and grooves appeared, and it relates to the material shrinkage (Fig. 2). Further details can be found in Ref. [5].

The real cause of stator vane damage was revealed by an experiment carried out on the power plant duty turbomachine in Vresova. There was an opportunity to carry out measurements during the gas turbine start-up following regular repairs. Two types of pressure probes were used during the measurement of nonsteady flow in the turbocompressor. Static pressure probes were located on the casing in planes 1, 2, and 3 (Fig. 1). Four total pressure probes were used in plane 4 at the rear of the EGV2 row. The probe diaphragm was cooled by water. The sensor was positioned in the middle of the vane pitch at a radial distance of 50 mm from the machine casing ($z/h=0.36$). Pneumatic probes were dynamically calibrated using the acoustic method [5].

Experimental investigation of nonsteady flows in the axial compressor was carried out in the working range of the gas turbine output of $P=55$ to 120 MW. In Fig. 3 the dependence of the compressor pressure ratio $\pi=p_{T4}/p_{TD}$ on the relative air mass flow rate (m/m_b) is shown. Compressor air flow rate is constant in the range of output $P=55-107$ MW. The inlet guide vanes have the constant stagger angle value of $\gamma_{\mathrm{IGV},b}=33$ deg. Syngas consumption grows with the gas turbine output. At higher outputs, $P>107$ MW, the air flow rate is increased due to the decrease in IGV stagger angle, as can be seen in Fig. 3. At the gas turbine output of $P=105$ MW the compressor working point is closer to the surge line than any other investigated points. Time dependent total pressure distribution in plane 4 and its amplitude/frequency characteristic are shown in Figs. 4(*a*) and 4(*b*) for the gas turbine output of $P=105$ MW. Amplitude value A was determined by the harmonic analysis of the pressure signal. In the case of the compressor working point, turbine output of 105 MW, we evaluated the maximum pressure amplitudes as $A=0.013$ MPa. Characteristic frequency of the flow pulsations $f=400$ Hz is apparent from the amplitude/frequency dependence shown in Fig. 4(*b*). First, the third and fifth natural frequencies of a probe impulse tube can be easily found. For the turbine output of $P=55$ MW the amplitudes values were approximately two times lower; $A=0.006$ MPa. For the maximum gas turbine output $P=118$ MW we measured lower pressure pulsations; $A=0.009$ MPa. If the natural gas would be

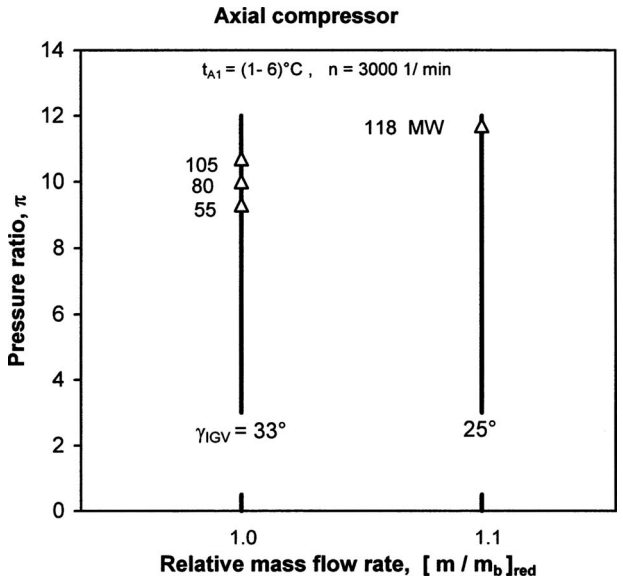

Fig. 3 Compressor characteristics

used as fuel, the flow pulsations amplitudes would be very low; $A < 0.002$ MPa.

The intensity of flow pulsations in the plane located at the rear of the compressor blading is dependent on the distance of the working point from the surge line. When the working point approaches the surge line, the area of separated flow enlarges on the vane suction surfaces of S17, EGV1, and EGV2. This phenomenon is accompanied by the vortex structure shedding from the vane surfaces, as will be revealed in Sec. 3.

Frequency of flow pulsations, found in the plane located at the rear of the compressor blading, $f = 380-400$ Hz for the turbine output of $P = 55-120$ MW is close to the first natural frequencies of the three last stator row vanes $f_1 = 325-345$ Hz. Stator vanes with rigid fixing of shanks in casing grooves can unusually exhibit cracks and ruptures due to the resonant effects.

Where the stator vane shanks fixing in casing grooves are not rigid, the high cycle fatigue damage was observed as no vane resonance can occur (Fig. 2). Such type of vane damage appeared more frequently than the vane rupture.

3 Numerical Study of the Unsteady Flow in Cascades

Numerical study of the unsteady flow in 2D cascades of the last three stator vane rows was carried out by the application of the FLUENT 6 code [16]. Cascades are located on the cylindrical surface, at a distance of 50 mm from the casing in the radial direction ($z/h = 0.36$). Total pressure probes located in the plane at the rear of EGV2 were installed at this radius (Fig. 1). The geometry of three considered stator cascades is known. This is not valid for moving cascade of 17th rotor row.

Flow in the inlet plane of 17th stator vane row was highly unsteady in three dimensions. Radial distribution of the flow properties is usually distorted, especially at high positive incidences of the blade elements. Effects of unsteady 3D flow structures due to the tip clearance flow and streamwise vorticity are ignored in this study. Also, the effect of upstream blade rows is not considered in the flow simulations. We can assume that results obtained by the numerical flow simulation in 2D cascade system will have qualitative meaning. However, we hope that they could contribute to a better understanding of flow pulsations origin.

3.1 Mathematical Model. The mathematical model is based on the system of Navier–Stokes equations for the turbulent flow of compressible fluid. For the turbulence model, standard RNG k-epsilon model is adopted. To find a suitable turbulence model in

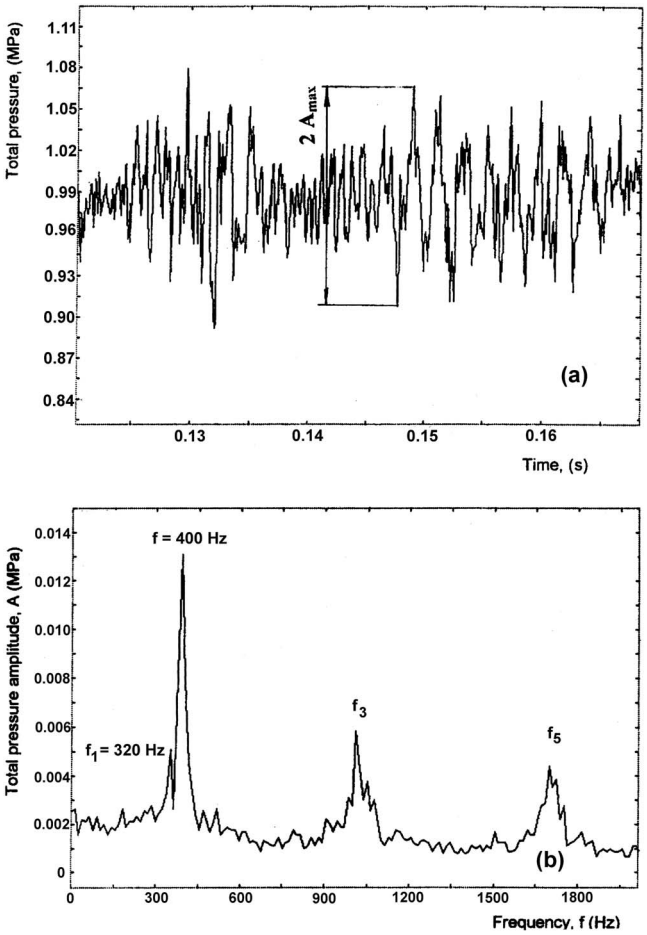

Fig. 4 (*a*) Total pressure in plane 4—*P*=105 MW and (*b*) amplitude/frequency characteristic of total pressure in plane 4—*P*=105 MW

computations of the unsteady separated turbulent flow is extremely subtle and difficult. Nonequilibrium wall functions defined in the FLUENT code [16] are used to model flow near the blade profiles. The numerical model is solved using the Runge–Kutta method in the form of finite volumes. A coupled implicit scheme with the second order accuracy and default under relaxation factors was applied. A five stage scheme with second order accuracy and fixed coefficients is used. Convergence is evaluated through the computations of residuals. At the end of each time step the residuals are of the order 10^{-6}.

Three types of 2D nonstructured computational grid (triangular, quadrilateral, and hybrid) were tested in a few cases of flow simulations in the investigated cascade system. The number of cells was changed in the range of 50,000–200,000. Obtained results proved that the numerical simulations are grid insensitive. Two-dimensional nonstructured computational mesh used in routine computations included 100,000 quadrilateral cells. The sliding mesh model was applied for the rotor/stator interaction to compute the unsteady flow field. Translational periodic boundary condition was used to model geometric periodicity of cascades [17].

3.2 Definition of Numerical Experiments. Three numerical experiments were carried out. In the first experiment (*Notation A*) the steady undisturbed flow with increased flow turbulence in the inlet plane of S17 stator cascade, $tu_1 = 3\%$, was considered. Increased turbulence was applied owing to the fact that the cascade system is located at rear of the multistage axial compressor. Reynolds and Mach numbers values of S17 cascade inlet flow were $Re_{in} = 1.3 \times 10^6$ and $Ma_{in} = 0.25$, respectively.

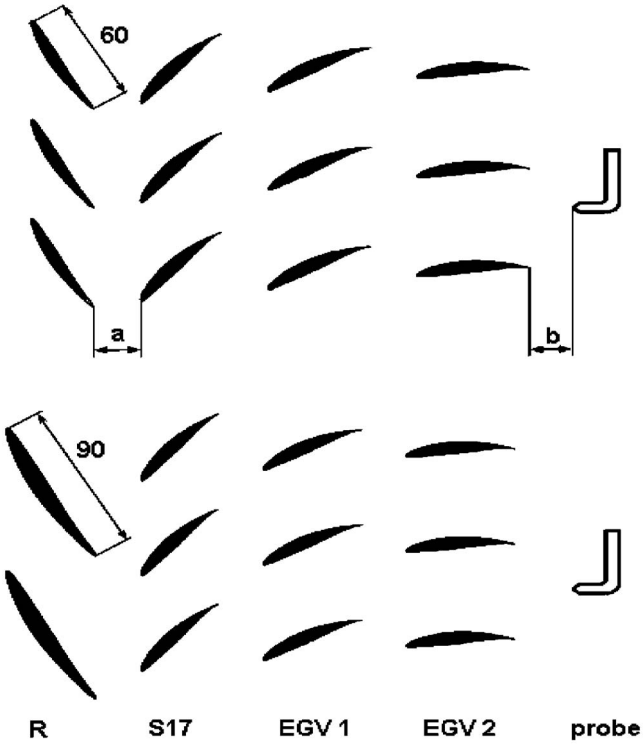

Fig. 5 Cascade system B1 and B2 a=24 mm, b=22 mm

The second computational experiment aimed to identify the effect of rotor/stator blade rows interaction (*Notation B*). Moving rotor cascade located upstream of the 17th stator cascade S17 was applied, see Fig. 5. Peripheral velocity of the rotor blades was 279.6 m/s. The exact geometry of 17th rotor cascade R17 was not known. For this reason new rotor cascade R was designed with the use of the Lieblein method [18]. Design of aerodynamic loading of both cascades (R, S17) was approximately the same ($D_R = D_{S17} = 0.46$). Unsteady flow fields were simulated for two variants of the rotor cascade—c_R=60 and 90 mm. Rotor blade pitch values were selected in agreement with suitable unsteady flow simulation conditions—B1, $s_R = s_{S17} = 57.5$ mm, and B2, $s_R = 3/2\, s_{S17} = 86.25$ mm. This refers to blade numbers ratios of $z_R/z_{S17} = 1.0$ and 2/3, respectively. Rotor blade wake passing frequency was f_{RB}=4860 and 3240 Hz, respectively. Turbulence intensity of the steady uniform undisturbed inlet flow of the rotor cascade was selected as $tu_1 = 3\%$; as in the first experiment. Several key parameters of the rotor R and S17 stator cascades are shown in Table 1. Axial distance between all cascades was a=24 mm (Fig. 5).

The third numerical simulation explores the sensitivity of different aerodynamic loading of the rotor R and S17 stator cascades on the formation of separated vortical areas on blade surfaces and their shedding in the flow direction. We considered higher aerodynamic loading of the S17 stator cascade (*Notation C).* Smaller variation in the aerodynamic loading of cascades can occur in the multistage compressor working at off-design conditions. Higher variation can be present in the case of the compressor mass flow rate regulation by the turning of the stator row vanes [19]. Two values of rotor cascade chord were applied as in the preceding case B.

Table 1 Cascades geometry for numerical experiments (NACA 65th Series Profile)

	c (mm)	s/c (1)	β_{L1} (deg)	β_{L2} (deg)	d/c (1)
Rotor R	60 (90)	0.958	67.8	49.7	0.100
S17	56.5	1.018	59.2	33.2	0.120
EGV1			39.2	13.2	
EGV2			18.6	−7.4	

Inlet components of the velocity, pressures, and temperatures of investigated cascade system are taken from a one-dimensional computation on the basis of experimental data recorded by the gas turbine measuring and control system. Exit static pressure values in the plane at the rear of the EGV2 row were obtained the same way.

Flow conditions in the inlet plane of the rotor cascade in second numerical experiments (B) are axial velocity w_{a1}=85 m/s, absolute flow angle α_1=40 deg, static temperature t_{s1}=311 °C, and air density ρ_{s1}=5.5 kg/m^3.

Reynolds and Mach numbers of inlet flow of rotor and S17 stator cascades are as follows:

(i) *Rotor cascade*. Ma_{1R}=0.47, blade chord c_R=60 mm, $Re_{1R} = 2.37 \times 10^6$, blade chord c_R=90 mm, and $Re_{1R} = 3.56 \times 10^6$.
(ii) *Stator cascade S17*. $Ma_{1,S17}$=0.34 and $Re_{1,S17} = 1.7 \times 10^6$.

The above data are valid for the design (reference) condition [18] of the rotor blade cascade. Increase in the incidence angles of the investigated cascades was carried out by means of the axial velocity decrease.

The variation in the aerodynamic loading of the rotor R and stator S17 cascades was achieved through the increase in the absolute flow angle value in the inlet rotor cascade plane experiments (*C*). This simulates turning of the stator vanes of the axial compressor 16th stage. In subsequent paragraphs the flow simulation results will be shown and discussed.

3.3 Flow Simulation Results in the Stator Cascade System: Numerical Experiment A. Unsteady flow fields in the original stator cascade system were computed for several inlet conditions of the S17 cascade: i_{S17}=0, 4, 6, 8, 10, 12, and 14 deg. Incidence angle value of i_{S17}=0 deg refers approximately to the compressor working conditions of the gas turbine using natural gas. Figures 6(*a*) and 6(*b*) show instantaneous vorticity magnitude fields in the investigated stator cascades at conditions with characteristic incidence angles of i_{S17}=8 and 12 deg. At condition i_{S17}=8 deg the flow is separated on the S17 and EGV1 suction surfaces, as it can be seen in Fig. 6(*a*). High vorticity values can be identified in the wake and flow separation areas of these cascades profiles. Practically the same vorticity patterns occur for the case of incidence angle of i_{S17}=10 deg. A low energy fluid with high vorticity due to stall was located in closed areas/bubbles, as shown in Fig. 6(*a*). Sudden change in the flow mechanism took place in the case of the incidence angle of i_{S17}=12 deg. Bubbles burst and large vortices were shed off in the direction of flow, S17, and EGV1 vane cascades. Vorticity values of the shed vortices decrease gradually owing to the flow dissipation in the direction of flow. This phenomenon can be observed in Fig. 6(*b*).

Figures 7 represents time dependent distributions of the effective vane force F_T for S17 vane profiles. Similar patterns were obtained for the EGV1 and EGV2 vanes. Significant flow pulsations do not exist in the cascade system at the incidence angle values of i_{S17}=0–10 deg according to the time dependent distributions in Fig. 7. Flow pulsations in the cascade system originated for higher values of S17 incidences of $i_{S17} > 12$ deg. This result is in a good agreement with the flow vorticity patterns shown in Figs. 6(*a*) and 6(*b*). Table 2 contains characteristic frequencies of the vane effective force's amplitude at two incidences i_{S17}=12 and 14 deg. In the case of the EGV1, two values of the characteristic frequency could be determined: basic and twice of the basic value. Total pressure probe data are also included in Table 2. It should be reminded that the total pressure probe was located at rear of the EGV2 (Figs. 1 and 5). Characteristic frequencies of the computed

a) $i_{S17} = 8^o$

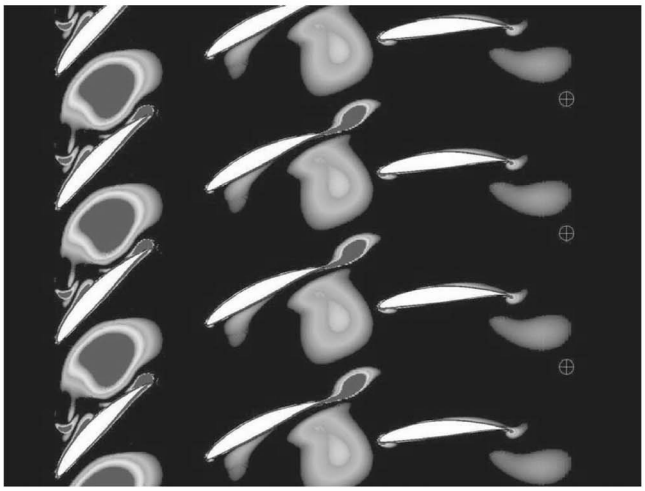

b) $i_{S17} = 12^o$

Fig. 6 Instantaneous vorticity patterns—(A)

time dependent flow properties were determined using harmonic analysis. It can be concluded, from each time dependent distribution, that the characteristic frequency of the effective vane forces of all cascades is identical for a given incidence angle i_{S17}. Frequency slightly increases with the incidence angle value i_{S17} increase as it can be seen in Table 2. Amplitudes of the total pressure are much higher in comparison with the experimental ones (A_p=0.013 MPa).

It should be added that the operating conditions of midspan blade elements in the rear part of the gas turbine axial compressor with extremely high incidence angles ($i_{S17}>12$ deg) cannot exist.

3.4 Flow Simulation Results in the Stator Cascade System: Numerical Experiment B. Basic description of the flow simulation results will be carried out for the flow case B1 ($s_R=s_{S17}$). Results of B2 ($2s_R=3s_{S17}$) vary only in a few aspects that will be discussed.

Flow case B1. Unsteady flow fields in the cascade system were computed for the several inlet conditions of the S17 cascade. We selected typical incidence angles values of i_{S17}=0, 4, and 7 deg. Incidence of i_{S17}=0 deg refers approximately to the compressor working conditions of the gas turbine using natural gas. Values of i_{S17}=4–7 deg may occur when the gas turbine output is P =60–105 MW (Fig. 3), and syngas is used as fuel.

Table 3 contains values of the inlet flow angles of the rotor $\alpha_{rel,1}$ and S17 stator cascades α_1 for the three conditions mentioned in the above text. Aerodynamic loading of the considered cascades can be judged on the basis of the incidence angle difference $\Delta i=i-i_{ref}$ and diffusion factor D [18]. These properties, included in Table 3, were computed on the basis of the flow simulations data. First, the average values of the flow properties along the vane pitch were determined according to the currently used relations in turbocompressor aerodynamics. Second, the time averaged values were computed. Flow on the suction surface of blade profile is stalled if $D>0.6$.

Figures 8(*a*)–8(*c*) show the instantaneous vorticity magnitude fields in the examined cascades with incidence angles of i_{S17}=0, 4, and 7 deg. Figure 9 shows the time averaged pitchwise distribution of the rotor exit absolute flow angle in the inlet S17 stator cascade plane. Examples of the time dependent distribution of the S17 vane effective forces are revealed in Fig. 10. The amplitude/frequency characteristic, shown in Figs. 11(*a*)–11(*d*), was obtained by the harmonic analysis of distribution valid for all cascades vane forces and total pressure in the EGV2 exit plane. Characteristic frequencies and the effective force amplitude of the rotor and S17 stator cascades are shown in Table 4 for the selected flow simulation variants.

(i) In the first variant of the flow simulation i_{S17}=0 deg, the aerodynamic loading of all cascades is low. Diffusion factor values of the rotor R and the S17 stator cascades are below the critical value [18]: D_R=0.46, D_S=0.48, see Table 3. We can observe flow without the significant flow separation on the suction surfaces of all cascades profiles in Fig. 8(*a*). Flow pulsations are relatively very low. Vane force amplitudes were less than A=0.001 MPa.

Lower velocity within the wake of the rotor blade profile leads to the higher incidence (inlet flow angle) of downstream of S17 stator vanes. This is documented by the pitchwise distribution of the time average absolute flow angle in Fig. 9. Angle value changed in the range of $\alpha_{1,S17}$=53 and 77 deg. If the rotor wake impinges the leading edge of downstream stator vanes, then it is chopped into two wake segments. Wake segments propagate independently from each other through the adjacent blades channels (Fig. 8(*a*)). They deform and decay during their downstream transfer. The mechanism, which determines the wake structure and decay, is viscous mixing, inviscid wake stretching, and negative jet effect, as can be found in Refs. [6,10,12,20]. It can be observed that the rotor wakes are mixed out in the EGV2 cascade. Due to the different length and orientation of the absolute velocity vectors of the wake and freestream, a slip velocity appears. The slip velocity stimulates the low momentum wake fluid to move along the wake segment from the blade profile suction side through the blade passage toward the pressure side of the adjacent blade profile. Near the suction side a high momentum enters the wake segment to replace fluid, which has moved across the blade passage. This process is termed as the negative jet wake effect; it has a strong influence on the unsteady profile velocity and pressure distribution on the cascade blade profile.

(ii) In the second investigated flow condition i_{S17}=4 deg (Table 3), the flow is slightly separated on the suction surface of the rotor blade and S17 stator vane profile (Fig. 8(*b*)). Separation point on the suction side is approximately 20% of the chord length from the trailing edge of both cascades, and vortices are produced in the separation region and are convected downstream. Separation vortices induce some counter-rotating vortices at the trailing edge. Vortices shed from the trailing edge with natural shedding vorticity and convect downstream. Diffusion factor values

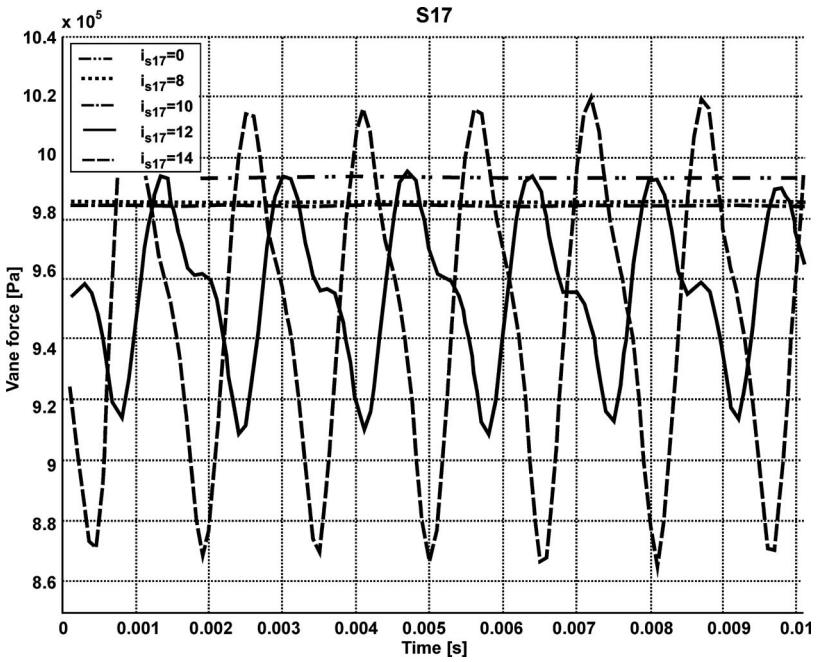

Fig. 7 Unsteady distribution of S17 vane force—(A)

are close to the critical value of $D_R=0.55$ and $D_{S17}=0.58$. Transfer of the wake segments in the S17 stator cascade blade passages can be observed. Wake segments contain vortices originated in the rotor cascade. The amount of the flow separation on the EGV1 profile is smaller than in comparison with the preceding stator cascade S17. Flow on the EGV2 profile is without visible separation. We can observe the periodic vane forces and the probe total pressure pulsations in Figs. 10 and 11. Characteristic values of the flow pulsations frequencies are $f=570$ and 2030 Hz with significant amplitudes. Total pressure amplitude is $A_p=0.008$ MPa, as can be seen in Fig. 11(*d*). It is evident that the stator cascade system flow pulsations are initiated by vortices shedding in the rotor cascade.

This can be explained by the effect of the rotor (R)/stator (S17) blade cascade's interaction. Due to the flow separation on the rotor blade suction surface, the increase in rotor wake width is observed. As a result of the rotor/stator blade row interaction the time averaged rotor pitchwise distribution of the inlet absolute flow angle exhibits higher amplitudes than in the preceding variant (Fig. 9). Shift of the transition point of the laminar boundary layer into the turbulent one, on the suction surface of S17 stator blade profile, occurred in the direction of the profile leading edge with the increase in the incidence angle [10]. Turbulent boundary layer separation point has the same tendency due to the higher positive pressure gradient on the profile suction surface. Shed vortices are contained in the rotor wake segments moving in the S17 stator cascade passage in the flow direction. The ratio of the rotor shed vortices f_R and blades passing frequency f_{RB} is $f_R/f_{RB}=0.12$.

The rotor shed vortice's dynamic effect on the unstable separated boundary layer seemingly causes shedding of the vortex structures from the S17 stator cascade profiles suction surfaces.

Table 2 Vane force amplitudes and frequencies (*A*)

i_{S17} (deg)	f (Hz)	Amplitude, A (MPa)			
		S17	EGV1	EGV2	Probe
12	590	0.042	0.025	0.047	0.038
14	645	0.073	0.022	0.071	0.085

Table 3 Flow simulations data (B1)

	Rotor, R				Stator, S17			
No.	$\alpha_{1,rel}$ (deg)	i (deg)	Δi (deg)	D (1)	α_1 (deg)	i (deg)	Δi (deg)	D (1)
1	68	0.2	0.8	0.46	59	0	1.1	0.48
2	71	3.2	3.8	0.54	63	4	5.1	0.58
3	74	6.2	6.8	0.64	66	7	8.1	0.65

$\Delta i=i-i_{ref}$.

(iii) Flow simulation results in the third flow simulation variant $i_{S17}=7$ deg exhibit strong flow separation on both rotor and stator cascade profiles. Diffusion factor values of the rotor and S17 cascades exceeded critical value $D_R=0.64$ and $D_{S17}=0.65$. Similar flow mechanism, as in the preceding flow regime, of the unsteady vortex flows can be observed as $i_R=3.2$ deg. Flow is separated at approximately a third of the chord length from the trailing edge of S17 cascade profiles (Fig. 8(*c*)). Vortices are produced in the separation region and then convected downstream. Amount of the flow separation area, on the suction profile surfaces of cascades EGV1 and EGV2, changes periodically as the consequence of the interaction of the unsteady vortex structures with the vane profiles. Rotor pitchwise distribution of the time averaged S17 stator inlet flow angle (Fig. 9) exhibits very large difference of the maximum and minimum values ($\alpha_{1,S17}=48-132$ deg). It means that in the wake there is reverse flow. Amplitude/frequency characteristic of the unsteady distribution for S17, EGV2 forces, and the probe total pressure shows the characteristic frequency value of $f=570$ Hz. The same result was obtained for the rotor cascade. In the case of EGV1 cascade the dominant frequency has values in the region of 800–850 Hz (Fig. 11(*c*)). This is caused by the

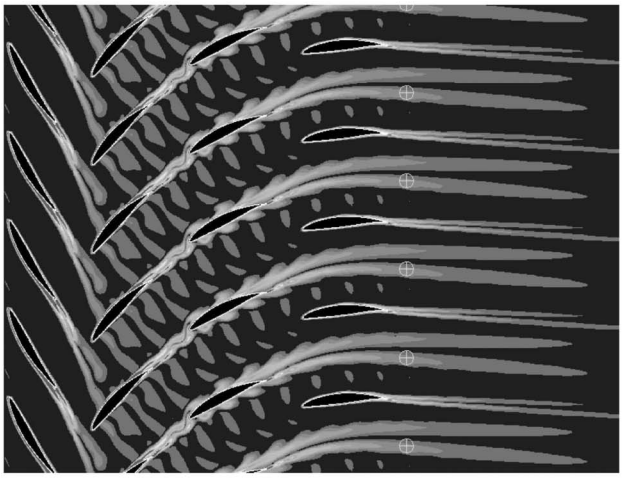

(a) $i_{S17} = 0^o$, (B1)

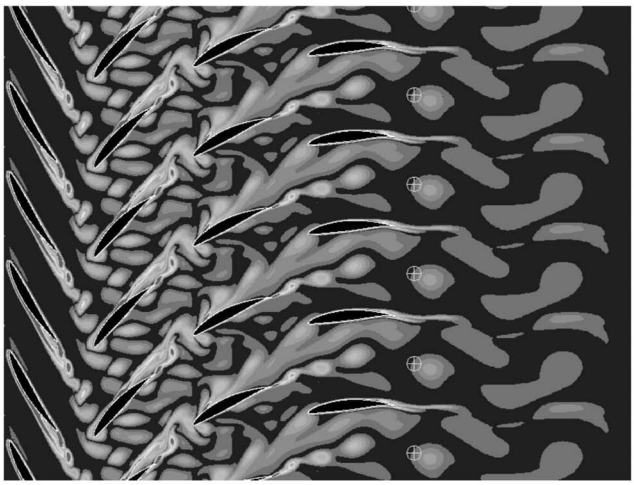

(b) $i_{S17} = 4^o$, (B1)

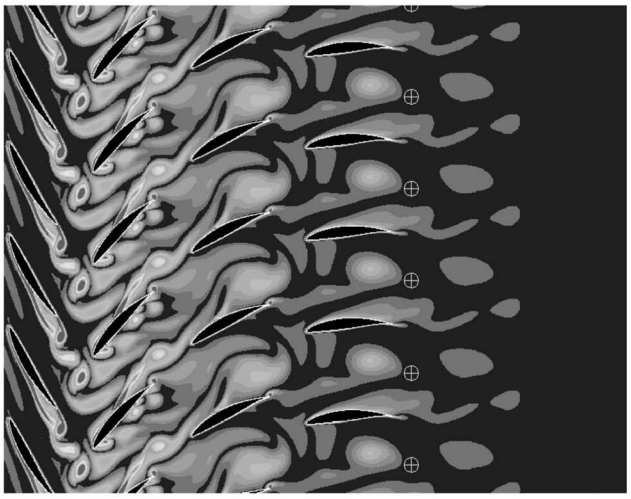

(c) $i_{S17} = 7^o$, (B1)

Fig. 8 (*a*) Instantaneous vorticity magnitude field—i_{S17} =0 deg, (B1); (*b*) instantaneous vorticity magnitude field—i_{S17} =4 deg, (B1); and (*c*) instantaneous vorticity magnitude field—i_{S17}=7 deg, (B1)

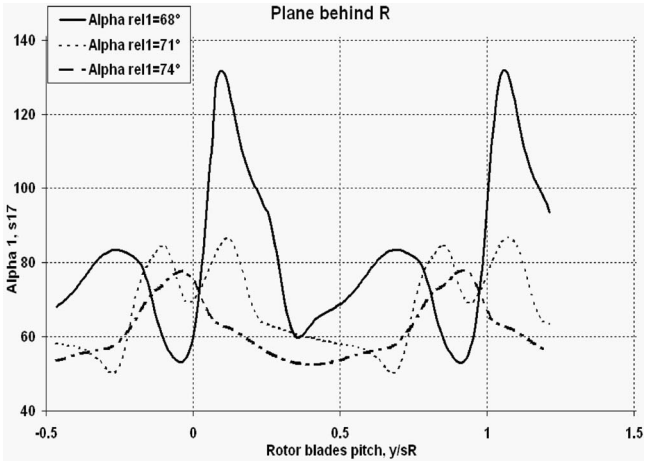

Fig. 9 Rotor pitchwise distribution of the time averaged absolute flow angle $\alpha_{1,S17}$ in the plane behind rotor

complex unsteady separated flow in the wake of the S17 cascade. Total pressure amplitude in the outlet plane of cascade EGV2 is A_p=0.028 MPa (Fig. 11(*d*)). It should be added that the amplitude of the S17 stator vane force is significantly higher than in the case of the rotor blade (Figs. 11(*a*) and 11(*b*)).

Flow case B2. Flow simulation results are similar to those valid for the flow case B1. Shedding of the vortices structure in the rotor cascade with length of c_R=90 mm started in the range of the rotor incidence angle of i_R=3.2–3.8 deg. In the simulation Variant 7, at an incidence of i_R=3.8 deg, weak pulsations appeared in the rotor cascade (Table 4). Figure 12 illustrates patterns of the vorticity magnitude field in the cascade system for Variant 8 with incidences of i_R=4.7 deg and i_{S17}=5.6 deg. Shed vortex systems from the rotor, S17 stator, and EGV1 cascades profiles, can be observed as in the flow case B1. The rotor/S17 stator counts ratio is 2:3. For that reason, within every second rotor R and third S17 stator passages identical periodical unsteady flow fields are found.

Main difference between results of the flow simulation of the B1 and B2 flow cases are in the values of the flow pulsations characteristic frequencies. For example, values of f_R=200 Hz and f_{S17}=80 and 200 Hz (Variant 8) are lower than values obtained for

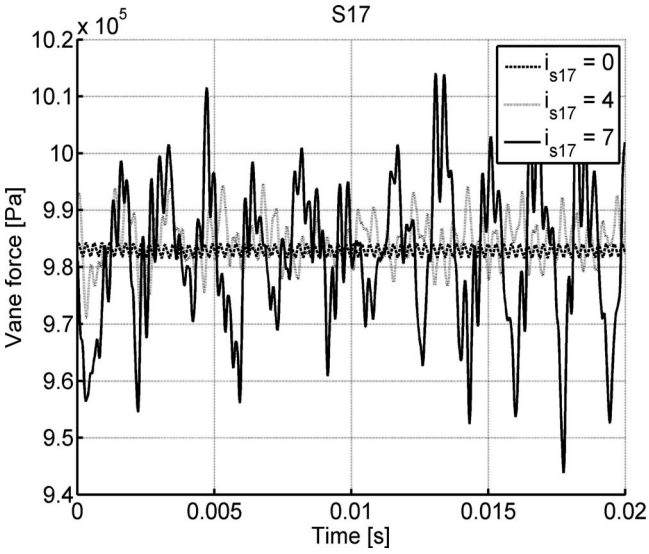

Fig. 10 Time dependent distribution of S17 vane force

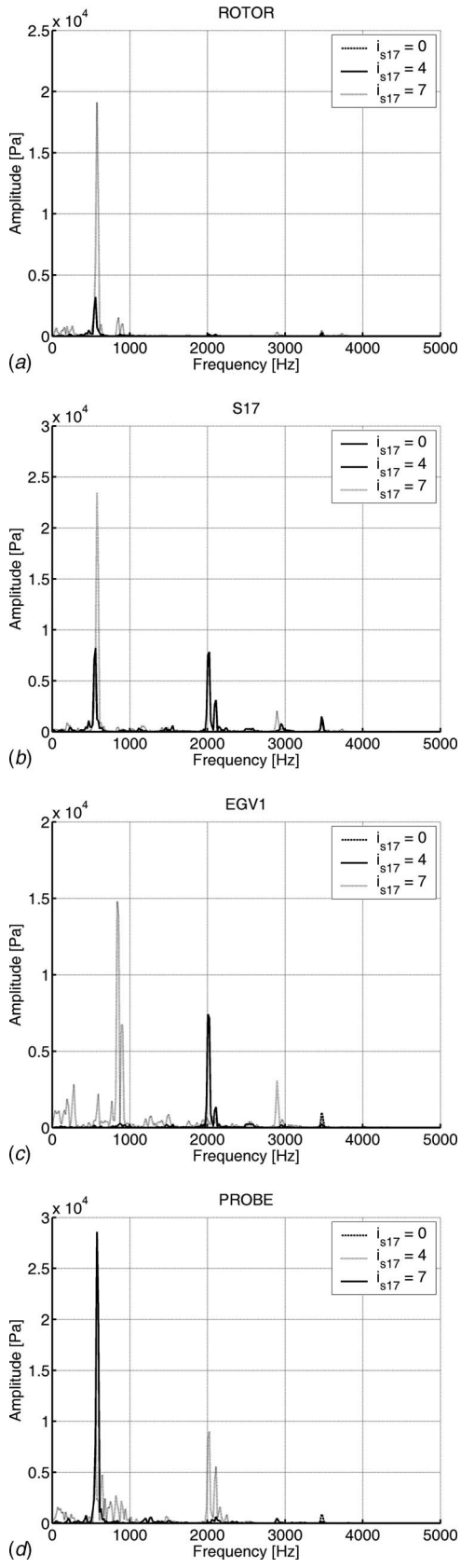

Fig. 11 (a) Amplitude-frequency characteristics of rotor blades forces—(B1), (*b*) amplitude-frequency characteristics of stator vanes forces—(B1), (*c*) amplitude-frequency characteristics of EGV1 forces—(B1), and (*d*) Amplitude-frequency characteristics of total pressure—(B1)

Table 4 Amplitudes and frequencies of periodic blade forces

				Rotor		Stator S17	
V		i_R (deg)	i_{S17} (deg)	f (Hz)	A (MPa)	f (Hz)	A (MPa)
1	c_R=60 mm	0.2	0	–	–	4860	0.001
2		3.2	4	570	0.003	570	0.0076
						2030	0.008
						4860	0.001
3	z_R/z_{S17}=1:1	6.2	7	570	0.014	570	0.023
						4860	0.001
4		2.8	6.8	–	–	2330	0.003
						2540	0.002
						4860	0.0015
5	c_R=90 mm	0.4	8.3	–	–	2250	0.004
						3240	0.0006
6		2.8	6.8	-	-	2330	0.002
						3240	0.0008
7	z_R/z_{S17}=2:3	3.8	5.7	1550	0.0015	90	0.002
						3240	0.0005
8		4.7	5.6	200	0.006	80	0.010
				1580	0.003	200	0.004
						3240	0.0015

the case B1—f_R=570 Hz and f_{S17}=570 Hz (Variant 3). This could be explained by use of the flow similarity criterion/Strouhal number defined as Sh=fc/w_1; w_1 and c are the inlet velocity and chord length, respectively. Although the flow similarity between B1 and B2 was not completely achieved, the trend in the relation between the shed vortices frequency f and cascade blade chord c could be valid, under the condition of constant velocity w_1.

3.5 Flow Simulation Results in the Stator Cascade System: Numerical Experiment C. Several simulations of the unsteady flow in a cascade system were performed at different values of the rotor R and S17 stator cascades incidences. The intention was to investigate flow separation mechanism on the suction surfaces of blade profiles at conditions when the aerodynamic loading of the S17 stator cascade was higher than in the case of the rotor cascade. For representation purpose, two combinations of incidence angle values were selected i_R=0.4 deg, i_{S17}=8.3 deg and i_R =2.8 deg, i_{S17}=6.8 deg, for the cascade systems with the rotor chord length of c_R=60 and 90 mm. Table 4 contains characteristic frequencies and amplitudes of the effective blade forces of the

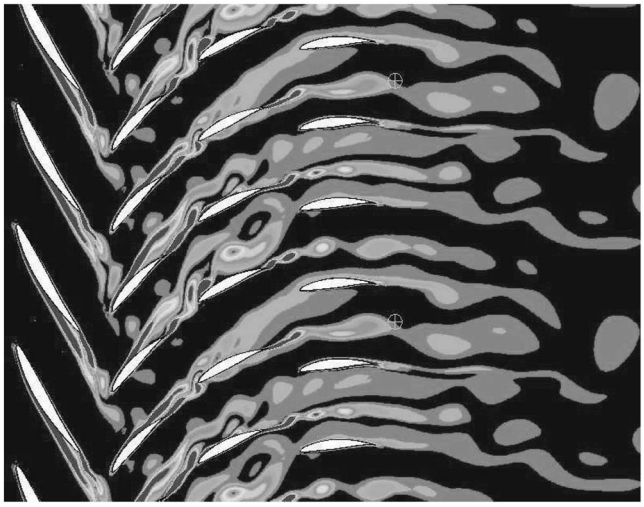

Fig. 12 Instantaneous vorticity magnitudes field i_R=4.7 deg, i_{S17}=5.6 deg, (B2)

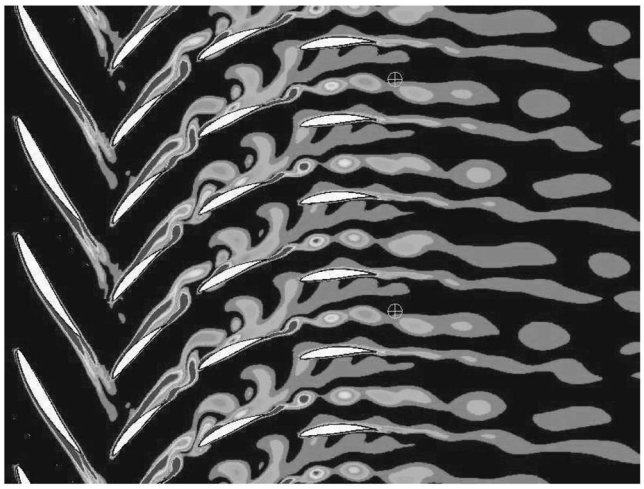

Fig. 13 Instantaneous vorticity magnitudes field i_R=2.8 deg, i_{S17}=6.8 deg, (B2)

rotor R and S17 blades profiles for Variants 4, 5, and 6.

Figure 13 shows vorticity magnitude patterns in a stator cascade system with the rotor cascade having chord length of c_R =90 mm at incidence angles of i_R=2.8 deg and i_{S17}=6.8 deg. Flow in the rotor cascade is without the boundary layer separation on the suction blade surface. Rotor wake segments in the S17 blade passage did not contain shed vortices with high vorticity. Boundary layer on the suction surface of the S17 stator vane profile is separated owing to the high incidence angle of i_{S17} =6.8 deg. However, the negative jet wake effect was not as strong as in the cases shown in Figs. 8(*b*) and 8(*c*) (B1), where the shed vortices were present in the rotor blade wakes. Characteristic frequency of the S17 stator blades force, excited by shedding of the vortex structures, f=2330 Hz is clear from Fig. 14(*b*). Stator blade force amplitude is A=0.002 MPa. Rotor blade passing frequency can also be found in Fig. 14(*b*). Similar results were obtained for another combination of incidence angles of i_R =0.4 deg and i_{S17}=8.3 deg (Table 4).

When the rotor cascade with shorter chord (c_R=60 mm) was used, located prior to the stator cascade system, we obtained results that did not vary from the data obtained for the variant with the longer rotor blade chord (Table 4). We point out that the rotor blade passing frequency value is f_{RB}=4860 Hz. It means that the effect of the rotor blade passing frequency value on the unsteady flows is not significant.

We can conclude, in the case of attached flow on the rotor cascade profiles surfaces, the flow separation in the stator cascade at high positive incidences exhibits high frequency of shed vortices f=2230–2550 Hz. S17 stator blade force amplitudes are relatively small A=0.002–0.004 MPa. These are significantly smaller than in the case of separated flow with vortex shedding in the rotor cascade. Differences can be seen in Figs. 14(*a*) and 14(*b*), where the amplitude/frequency characteristic for the flow simulation variants with the same and different aerodynamic loading the of rotor R and S17 stator cascades are shown.

3.6 Comparison of Experimental and Numerical Flow Simulation Results. Experimental data comparison of flow pulsations in investigated gas turbine axial compressor and unsteady flow simulation results in 2D cascade system can be carried out only for the case of the total pressure in the plane at the rear the EGV2, where the total pressure probe was located (Figs. 1 and 5). Values of the flow pulsations frequencies and amplitudes are shown in Table 5. Simulation data of the numerical experiment B are used; refer to Variants 2, 3, and 8 shown in Table 4. Measured

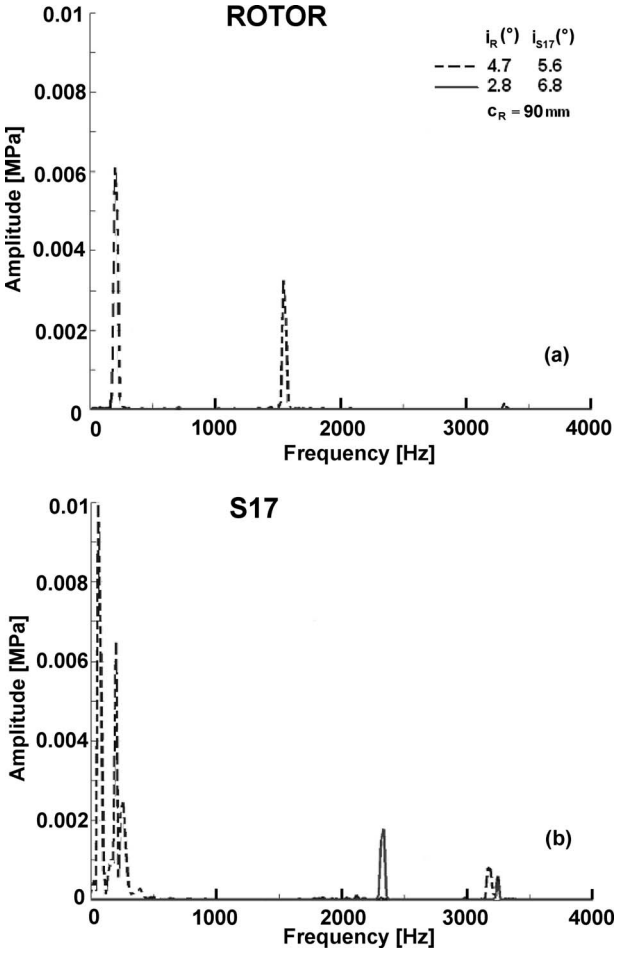

Fig. 14 Amplitude-frequency characteristics of rotor R and S17 blade forces—(B2)

data relate to the gas turbine output of 105 MW.

Prior to making comparison we should repeat significant assumptions used in flow simulations in 2D cascade system. Leakage flows over the blade tips and underneath the stator attachments, occurring near end walls, are ignored. The same applies for air flows extraction for cooling purposes. These phenomena apparently influence vortices shedding due to the flow separation on blade profiles. The influence of upstream blade rows is also not considered in the flow simulations. Significant uncertainty is associated with unknown geometry of 17th rotor blade row. For such reason new rotor blade cascade was designed with two values of blade chord: c_R=60 and 90 mm. The real value is somewhere in this range, as can be deduced from the compressor blading scaled drawing.

Data analysis in the preceding text presents, that the rotor and

Table 5 Total pressure behind EGV2 (z/h=0.36)

Var.		i_{S17} (deg)	f (Hz)	A_p (MPa)
	Experiment GT: P=105 MW		400	0.013
	Simulation			
2	B1: c_R=60 mm	4	570	0.008
3		7	570	0.028
8	B2: c_R=90 mm	5,6	80	0.007
			170	0.004

stator blade elements of the 17th stage work in the gas turbine output of 105 MW at incidences: $i=3-7$ deg. In consequence we can state that the experimental total pressure amplitude $A_p=0.013$ MPa only qualitatively agrees with values obtained with the aid of numerical flow simulations, as can be seen in Table 5. Experimental flow pulsation frequency value of $f=400$ Hz is in the range derived from the numerical flow simulation data $f=80-570$ Hz. Such result can be explained by the above mentioned uncertainty and assumptions and the latest developments in the unsteady separated flow modeling.

4 Conclusions

Blade failures in the rear part of the gas turbine axial compressor frequently occur if low calorific fuel is used. In such case the working point of a compressor is moved to the stability limit. Blade elements of last blade rows work at higher positive incidence angles, and the flow separation on the blade suction surfaces occurs. There is a theory that flow pulsations are caused by shedding of separated vortex structures from the suction surfaces of blade profiles.

Presence of the flow pulsations in the rear part of the seventeen stage axial compressor of GE 9001E gas turbine Alstom, located in Vresova power plant, was experimentally proven. Syngas derived by the brown coal gasification was used as fuel. Typical frequency of the flow unsteadiness was $f=380-400$ Hz. Amplitude of the time dependent total pressure distribution in the compressor blading exit plane grew with the shift of the operating point away from the design point. However, the flow pulsations frequency was approximately constant. Maximum value of the total pressure amplitude was $A_p=0.013$ MPa.

Three numerical experiments, denoted by A, B, and C, were carried out for the explanation of the flow pulsation origin in the axial compressor last three stator rows. Flow simulations were carried out in the 2D cascade system in the middle part of annulus height ($z/h=0.36$). Inlet flow parameters were determined using the gas turbine control system data. Real flow in the multistage axial compressor blading is very complicated. It was anticipated that results of the flow simulations in 2D cascade system could help to better understanding of the investigated phenomena.

Experiment A was devoted to the flow simulations of steady undisturbed inlet flow. High flow turbulence intensity was used; $tu_1=3\%$. Periodic effective vane forces of the investigated cascades appeared at a relatively high incidence angle of S17 cascade of $i_{S17}=12$ deg. However, such working condition cannot exist at the rear stages in a multistage axial compressor. It can be stated that the appearance of the flow pulsations in our cascade system is evidently connected with the rotor/stator blade rows interaction.

For such reason a rotor cascade, located in front of S17 cascade, was designed. Identical aerodynamic loading of both cascades was used. Diffusion factor value was $D_R=D_{S17}=0.46$. Two values of the rotor chord length ($c_R=60$ and 90 mm) were applied in order to simulate two ratios of rotor and stator S17 cascades; 1:1 and 2:3. Rotor blades passing frequency values were $f_{RB}=4860$ and 3240 Hz, respectively

Second (B) of the numerical simulation experiments had the same aerodynamic loading of the rotor R and S17 stator cascades. The flow mechanism description, rotor/stator S17 blade's ratio of 1:1, was a chord length of $c_R=60$ mm—flow case B1. At the rotor cascade, when the incidence angle is greater than $i_R=3.2-3.5$ deg, the flow separation appeared on the suction blade surface with shedding of vortex structures in the flow direction. Characteristic frequency of $f=570$ Hz was found. In the stator S17 cascade shedding of vortices was more intensive with the same frequency. This can be explained by the rotor wake/stator S17 cascade interaction. Rotor wake segments moving in the S17 stator cascade passage contained vortices, which acted on the separated boundary layer on the suction vane surface and initiated formation of vortices and their shedding. Complex unsteady flows could be observed in the first exit guide vane (EGV1) cascade passages. Interaction of decayed vortices from S17 cascade and new, which originated in EGV1, occurred. Flow in EGV2 cascade was without separation. In EGV2 cascade passage one could find dissipation of vortex structures in the flow direction.

If incidence angles of both rotor R and S17 stator cascades are increased, then amplitudes of the periodic blade forces and flow parameters will grow.

Outcome of the flow simulation with the longer rotor chord ($c_R=90$ mm, ratio of blades numbers 2:3—flow case B2) exhibits the same flow mechanism of the unsteady flow as in the case of the shorter blade chord (B1). Two/three typical frequencies were found in the amplitude-frequency dependencies of the periodic blade forces $f=80$, 200 Hz. Values are lower than in the case of B1 results. This can be linked to the rotor/stator blades counts ratio of 2:3 and equally to the flow law valid for the unsteady flows expressed by the Strouhal number.

The last of the numerical experiments (C) investigated different aerodynamic loadings of the rotor R and S17 cascades. Incidence angles of the rotor cascade had a lower value than the stator S17 cascade. If the flow was attached on the suction blade surface of rotor cascade, then the flow separation in stator cascade at high positive incidences exhibited a high frequency of shedding vortices in the range of $f_{shed}=2200-2300$ Hz. Amplitudes of the stator vane force S17 were smaller than in the case of the unsteady separated flow in rotor cascade.

Experimental values of the total pressure amplitude $A_p=0.013$ MPa and frequency $f=400$ Hz in the compressor blading exit plane at the gas turbine output of 105 MW are in qualitative agreement with the values of the flow simulation results of the numerical experiment (B). Such conclusion can be explained by assumptions used in our computations and the latest developments in flow modeling of the unsteady separated flow in turbomachine aerodynamics.

Acknowledgment

Research was supported by the Grant Agency of the Czech Republic—Grant Nos. 101/05/1148 and IAA200760801 and by the Sokolovska Coal Co. a.s.

Nomenclature

- A = amplitude
- c = chord
- F_T = effective vane force $F_T=1/s\int p_T ds$
- D = diffusion factor
- d = maximum blade profile thickness
- f = frequency
- h = blade height
- i = incidence angle
- m = mass flow rate
- P = gas turbine output
- p_T = total pressure
- s = blade pitch coordinate along profile surface
- t_{A1} = inlet air temperature
- w = velocity
- z = radial distance from casing, number of blades
- α = flow angle
- β = blade angle
- γ = stagger angle

References

[1] Bucko, Z., Engelhard, W. J., and Vierrath, H., 1999, "400 MWe IGCC Power Plant With the HTW Gasification in the Czech Republic," Gasification Technologies Conference, San Francisco, CA, Oct. 17–20.

[2] Huth, M., Heilos, A., and Gaio, G., and Karg, J., 2000, "Operation Experiences of Siemens IGCC Gas Turbines Using Gasification Products From Coal and Refinery Residues," ASME Paper No. 2000-GT-26.

[3] Cyrus, V., Rehak, K., and Najvar D., 2004, "Operational Experience of the ALSTOM Gas Turbine Compressor in the Gasification Combined Cycle Using

Brown Coal in Vresova," XXXVI. Kolloquium Dresden, Tagungsband II, Vortrag No. 31.
[4] Ferreira, S. B., and Do Nascimento, M. A. R., 2007, "Gas Turbine Engine Off—Design Performance Simulation Using Syngas From Biomass Derived Gas as Fuel," ASME Paper No. GT2007-27804.
[5] Cyrus, V., Rehak, K., and Polansky, J., 2006, "Unsteady Flows in the Last Stator Rows of Axial Compressor of Gas Turbine Working in Gasification Combined Cycle," ASME Paper No. GT 2006-90202.
[6] Tan, C., 2006, "Unsteady Flows in Compressors," *Effects of Aerodynamic Unsteadiness in Axial Turbomachines* (Lecture Series 2005-03), Von Karman Institute for Fluid Dynamics, Brussels.
[7] Valkov, T., and Tan, C. S., 1999, "Effect of Upstream Vertical Disturbances on the Time Averaged Performance of Axial Compressor Stators: Part 1—Framework of Technical Approach and Wake-Stator Blade Elements," ASME J. Turbomach., **121**, pp. 377–386.
[8] Storer, J. A., and Cumpsty, N. A., 1991, "Tip Leakage Flow in Axial Compressors," ASME J. Turbomach., **113**, pp. 252–259.
[9] Cumpsty, N. A., 1989, *Compressor Aerodynamics*, Longman Group UK Limited, London.
[10] Mailach, R., and Vogeler, K., 2006, "Blade Row Interaction in Axial Compressors. Part I: Periodical Unsteady Flow Field, Part II: Unsteady Behaviour of Boundary Layer, Pressure Distribution and Excited Pressure Force of Compressor Blades," *Advances in Axial Compressor Aerodynamics* (Lecture Series 2006-06), Von Karman Institute for Fluid Dynamics, Brussels.
[11] Adamczyk, J. J., and Celestina, M. L., 1993, "The Role of Tip Clearance in High Speed Fan Stall," ASME J. Turbomach., **115**, pp. 28–39.
[12] Stauter, R. C., Dring, R. P., and Carta, F. O., 1991, "Temporally And Spatially Resolves Flow in Two-Stage Axial Compressor. Part I—Experiment," ASME J. Turbomach., **113**, pp. 212–226.
[13] Mayle, R. E., 1991, "The Role of Laminar-Turbulent Transition in Gas Turbine Engines," ASME J. Turbomach., **113**, pp. 509–537.
[14] Walker, G. J., Hughes, J. D., Kohler, I., and Solomon, W. J., 1999, "Periodic Transition on an Axial Compressor Stator: Incidence and Clocking Effects: Part I: Experimental Data, Part II. Transition Onset Predictions," ASME J. Turbomach., **121**, pp. 398–415.
[15] Trebinjac, I., Charbonnier, D., and Leboeuf, F., 2005, "Usteady Rotor-Stator Interaction in High Speed Compressor and Turbine Stages," J. Therm. Sci., **14**, pp. 289–297.
[16] FLUENT 6 Manual.
[17] Knorek, J., 2007, "The Methodology of Simulations of Tubes Array Vibrations in a Cross-Flow," Ph.D. thesis, ZCU University, Pilsen.
[18] Lieblein, S., 1966, "Experimental Flow in Two-Dimensional Cascades," pp. 183–226, NASA Report No. SP 36.
[19] Cyrus, V., 1998, "Aerodynamic Performance of an Axial Compressor Stage With Variable Rotor Blades and Stator Vanes," ASME Paper No. 98-GT-151.
[20] Zheng, X.-Q., Zhou, X.-B., and Zhou, S., 2004, "Investigation on a Type of Flow Control to Weaken Unsteady Separated Flows by Unsteady Excitation in Axial Flow Compressors," ASME Paper No. GT2004-53167.